

Journal of
Mechanics of
Materials and Structures

**NUMERICAL SIMULATION OF TSUNAMI PROPAGATION USING
THE CHARACTERISTIC-BASED SPLIT METHOD**

Gunawan Budi Wijaya, Tam Thanh Bui and Worsak Kanok-Nukulchai

Volume 3, N° 10

December 2008



mathematical sciences publishers

NUMERICAL SIMULATION OF TSUNAMI PROPAGATION USING THE CHARACTERISTIC-BASED SPLIT METHOD

GUNAWAN BUDI WIJAYA, TAM THANH BUI AND WORSAK KANOK-NUKULCHAI

A disastrous tsunami struck North Sumatra, Indonesia and many other countries on December 26, 2004. In response to this disaster, we develop a two-dimensional numerical model to simulate tsunami propagation on the open sea. Tsunami propagation — a process during which the wave has a relatively small height compared to its breadth — is modeled using the shallow water equations. To solve these equations, our model employs the characteristic-based split method first introduced by Zienkiewicz. Four case studies are proposed to verify the numerical model, and our results show that the present numerical model is both accurate and efficient. The numerical model is then used to model the propagation of the tsunami of December 26, 2004, and gives a relatively close result.

1. Introduction

During the last decades, several tsunamis have occurred, striking coastlines and causing devastating property damage and loss of life. The 1992 Flores Tsunami killed more than 264 people in Indonesia, the 1993 Hokkaido tsunami in Japan killed 239 people. One of the worst on record is the December 26, 2004 tsunami, which struck North Sumatra, Indonesia and many other countries, killing more than 289,000 people.

Basically, tsunami can be generated when the sea floor abruptly deforms and vertically displaces the overlying water. Earthquakes are the most frequent triggers, although in some cases a tsunami is generated by a landslide, volcanic eruption, explosion, or the impact of a meteorite or asteroid. When an earthquake occurs beneath the sea, it can cause the water above the deformed area to displace from its equilibrium position. Waves are formed as the displaced water mass, under the influence of gravity, moves to regain its equilibrium. When a large enough area of the sea floor suddenly changes elevation, a tsunami forms.

Tsunami propagation on the open sea is characterized as a shallow-water wave with long period and small height compared to its breadth. Shallow-water waves move at a speed that is equal to the square root of the product of the acceleration of gravity (9.8 m/s^2) and the water depth. Thus, the deeper the water, the faster the wave. And since waves lose energy at a rate inversely related to their wavelength, tsunami can travel at high speeds for long periods of time, losing very little energy in the process. As a tsunami leaves the deep water of the open ocean and travels into shallower water near a coast, it transforms. The tsunami's energy flux, which is dependent on both its wave speed and wave height, remains nearly constant. Consequently, as the tsunami travels into the shallower water, its speed is reduced and its height

Keywords: tsunami propagation, shallow water equations, finite element method, characteristic-based split method.

The authors acknowledge support from the Royal Thai Government Joint Research Program, which has provided funds for *Tsunami Tracking and Alert System* projects.

grows. As a result, tsunamis grow to be several meters or more in height near the coast, and may appear as a rapidly changing tide, a series of breaking waves, or even a bore.

When a tsunami reaches land, it will start to lose some energy due to reflection from the shore, bottom friction, and turbulence. Although there are energy losses, many tsunami waves don't break. They simply surge, flooding low-lying areas, and destroying vegetation, houses, and other coastal structures before rebounding off of cliffs or hills. Often, this flow back into the ocean causes as much damage as the initial onslaught.

This physical phenomenon of tsunami propagation can be mathematically modeled using the Shallow Water Equations (SWE), which are based on the Navier–Stokes equations. In the early days of using computers to find the numerical solutions of fluid flows, finite difference methods were the main tools used by researchers. Various finite difference models have been developed for tsunami wave propagation analysis, such as FUNWAVE, which was developed based on the extended Boussinesq model [Wei and Kirby 1995], TUNAMI which uses linear shallow water theory in a spherical coordinate system [Imamura 1996], SWAN, a model for shallow water and long waves, ZUNI, which uses a two dimensional incompressible Navier–Stokes formulation, and SOLA-3D, a three dimensional incompressible Navier–Stokes model for solving water wave problems of all types. Numerous examples and discussion on the applications of SWAN, ZUNI and SOLA-3D models are presented in [Mader 2004].

In recent years, finite element methods have been widely considered as an alternative choice to finite difference methods because of their flexibility in accurately representing arbitrary topography and complex boundary conditions. Several finite element models have been formulated to study shallow water wave propagation. Grotkop [1973] presents a space-time finite element model for long-period water wave analysis, however this model requires more computer storage and running time than an explicit difference model. For tsunami analysis, Houston [1978] uses a hybrid finite element method to study the interaction of tsunamis with the Hawaiian Islands. Sklarz et al. [1979] simulated the November 29, 1975 tsunami that hit the Hawaiian Islands. Considerable effort has been devoted to improving the performance of finite element models. In the realm of time integration techniques, Kawahara et al. [1978] implemented a two step explicit method which is modified from the Lax–Wendroff finite difference method. Malone and Kuo [1981] proposed semiimplicit time integration schemes that allow the choice of a time step based on accuracy, rather than some Courant-type restriction. Peraire et al. [1986] presented a general explicit formulation which requires little computer storage and can be used on mini- and microcomputers.

The main difficulty of using finite element methods for flow problems is due to the convection terms in the governing equations of fluid. The solutions of convection-dominated problems are often destroyed by spurious oscillations if certain parameters exceed a critical value. Severe mesh and time step refinement are required to remove these oscillations. Zienkiewicz and Codina [1995] introduced a new finite element algorithm which precludes oscillations without the requirement of mesh or time step refinement. This finite element algorithm is named the *characteristic-based split* (CBS) method, and combines the characteristic Galerkin method to deal with advection-dominated flows with a splitting technique to make the system equations become self-adjoint. Such a system of equations can be solved optimally by using the Galerkin formulation. In semiimplicit form, the algorithm requires a critical time step dependent only on the current velocity rather than on the wave celerity. Many studies using the CBS method have been conducted to solve more general fluid problems [Zienkiewicz et al. 1999; Nithiarasu et al. 2004; Ortiz

et al. 2004]. Here, the CBS method is used to develop a two-dimensional numerical model to simulate the propagation of the December 26, 2004 tsunami.

2. Review on shallow water equations

The governing equations for general fluid dynamics problems are the Navier–Stokes equations, which are derived from fluid’s characteristic conservation of mass and momentum, as shown below:

Continuity Equation:
$$\frac{\partial \rho}{\partial t} + \frac{\partial}{\partial x_i}(\rho u_i) = 0 \tag{1}$$

Momentum Equation:
$$\frac{\partial(\rho u_i)}{\partial t} + \frac{\partial}{\partial x_j}[(\rho u_i)u_j] - \frac{\partial}{\partial x_j}[\tau_{ji}] + \frac{\partial p}{\partial x_i} + Q_i = 0, \tag{2}$$

where $i, j = 1, 2, 3$ represent the coordinate directions, ρ is the water density, u_i is the velocity vector, p is the water pressure, and Q_i is a source vector term that includes Coriolis force, surface and bottom shear stresses, and atmospheric gradient.

2.1. Shallow water flow characteristic. Shallow water flow is a nearly horizontal flow. This allows a considerable simplification in the mathematical formulation and numerical simulation allowing the assumption that the pressure distribution is hydrostatic. However, shallow water flow is not exactly two-dimensional. Density stratification due to differences in temperature or salinity cause variations in the vertical direction. In many shallow water flows, these three-dimensional effects are not essential and it is sufficient to consider the depth-averaged form, which is two-dimensional in the horizontal plane.

The basic assumption in shallow-water theory is that vertical scales are much smaller than horizontal ones. The vertical parameters include the water depth H , the variation in the bottom level, and the variation in water height h . The horizontal ones include the physical dimensions of the basin (length, width) and the wavelength λ (Figure 1). From linear wave theory, the ratio of water depth to wavelength must be less than about 0.05 [Le Méhauté 1976]. This can be considered as the upper limit of shallow water theory. In shallow water flow, the horizontal velocities are of primary importance, and are defined

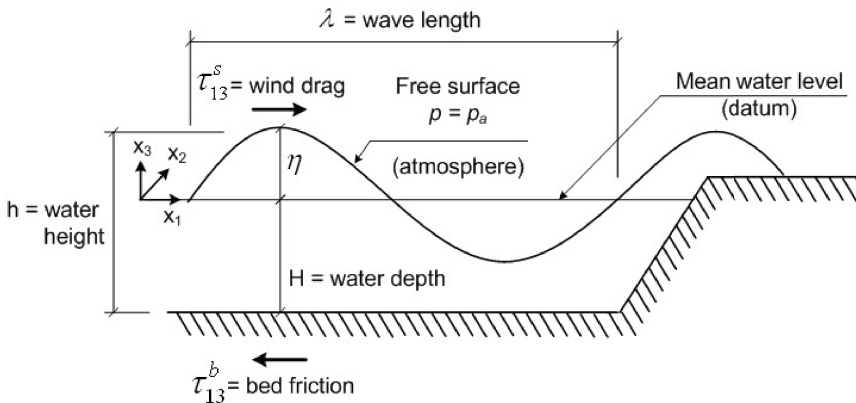


Figure 1. Shallow water flow profile.

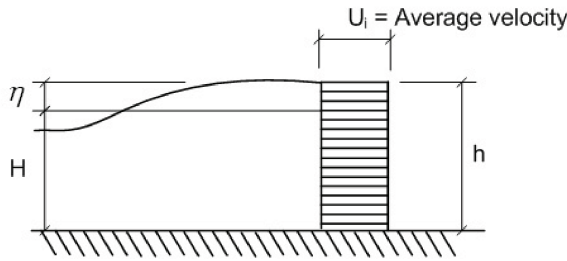


Figure 2. Velocity distribution of shallow water flow.

as the average velocity:

$$\int_{-H}^{\eta} u_i dx_3 = U_i(H + \eta) = U_i \cdot h, \tag{3}$$

where U_i is the average velocity vector (Figure 2).

In general shallow water flow, there are two types of boundary conditions governing the fluid at its top and bottom:

- A kinematic boundary condition, which states that water particles cannot cross either boundary, further requires that,
 - along the solid bottom ($z = -H$), velocities normal to the surface must vanish:

$$-u_1 \frac{\partial H}{\partial x} - u_2 \frac{\partial H}{\partial y} - u_3 = 0, \tag{4a}$$

- along the free top surface ($z = \eta$), since the surface must not move away from itself, the fluid's relative normal velocity must vanish:

$$\frac{\partial \eta}{\partial t} + u_1 \frac{\partial \eta}{\partial x} + u_2 \frac{\partial \eta}{\partial y} - u_3 = 0. \tag{4b}$$

- A dynamic boundary condition, which defines the forces acting at each boundary:
 - Along the bottom, it is assumed that the viscous fluid sticks to the surface (no slip condition):

$$u_1 = u_2 = 0. \tag{4c}$$

- Along the top, it is assumed that the stress in the fluid just below the free surface is the same as that in the air just above, namely the atmospheric pressure:

$$p = p_a. \tag{4d}$$

2.2. Shallow water continuity equation. The equation for the free surface is derived by an integration of the continuity equation (1) over the depth coordinate x_3 :

$$\int_{-H}^{\eta} \frac{\partial u_1}{\partial x} dz + \int_{-H}^{\eta} \frac{\partial u_2}{\partial y} dz + \int_{-H}^{\eta} \frac{\partial u_3}{\partial z} dz = 0. \tag{5}$$

By using the Leibniz rule of integrals, Equation (5) can be written as

$$\frac{\partial h}{\partial t} + \frac{\partial(hU_j)}{\partial x_j} = 0. \tag{6}$$

With $j = 1, 2$, Equation (6) can also be written as

$$\frac{\partial h}{\partial t} + \frac{\partial(hU_1)}{\partial x} + \frac{\partial(hU_2)}{\partial y} = 0. \tag{7}$$

2.3. Shallow water momentum equations. In shallow water flow, the vertical velocity (u_3) is very small, and the corresponding acceleration can be neglected. So the vertical momentum equation becomes:

$$\frac{1}{\rho} \frac{\partial p}{\partial x_3} + g = 0. \tag{8}$$

After integration, we can determine the pressure as

$$p = \rho g(\eta - z) + p_a. \tag{9}$$

The other momentum equations for horizontal velocities are also integrated over the depth:

$$\int_{-H}^{\eta} \left[\frac{\partial(u_i)}{\partial t} + \frac{\partial}{\partial x_j}(u_i u_j) + \frac{1}{\rho} \frac{\partial p}{\partial x_i} - \frac{1}{\rho} \frac{\partial \tau_{ji}}{\partial x_j} - Q_i \right] dx_3 = 0. \tag{10}$$

Using the definition of p from Equation (9), and with $i = 1, 2$, Equation (10) can be written as the conservative form of the depth-averaged equations:

$$\begin{aligned} \frac{\partial(hU_i)}{\partial t} + \frac{\partial}{\partial x_j} \left[(hU_i U_j) + \delta_{ij} \frac{1}{2} g(h^2 - H^2) \right] \\ + \frac{\partial}{\partial x_j} \left[-\frac{h}{\rho} \bar{\tau}_{ji} \right] + \left[-\frac{1}{\rho} (\tau_{3i}^s - \tau_{3i}^b) - hfi - g(h - H) \frac{\partial H}{\partial x_i} + \frac{h}{\rho} \frac{\partial P_a}{\partial x_i} \right] = 0. \end{aligned} \tag{11}$$

The term τ_{ij}^s is the surface shear stress which is caused by the wind stress. The magnitude and direction of the wind stress on the sea surface are determined by the flow in the atmosphere. A semiempirical formula to calculate the magnitude of the wind stress is given by Gill [1982] as

$$\tau_{ij}^s = c_d \cdot \rho \cdot W_i^2, \tag{12}$$

where

$$c_d = \text{drag coefficient} \quad \text{and} \quad W_i = \text{wind speed}.$$

The term τ_{ij}^b is the bottom shear stress due to the no-slip boundary condition. This stress is influenced by the roughness of the bottom layer. A simple approximation to calculate this bottom stress is given by Groen and Groves [1962] as

$$\tau_{3j}^b = c_f \cdot \rho \cdot |U| U_i, \tag{13}$$

where

$$|U| = \sqrt{U_i U_i} \quad \text{and} \quad c_f = \text{standard friction coefficient}.$$

The term $\partial P_a/\partial x_i$ is the atmospheric pressure gradient. This may be important for the simulation of storm surges [Heaps 1967]. The value of this gradient can be obtained, for example, from a meteorological forecast.

2.4. Shallow water equations. From the continuity and momentum equation, the complete form of the Shallow Water Equations can be written in the conservative forms as

$$\frac{\partial \Phi}{\partial t} + \frac{\partial F_i}{\partial x_i} + \frac{\partial G_i}{\partial x_i} + Q = 0, \tag{14}$$

where

$$\begin{aligned} \Phi &= \begin{bmatrix} h \\ hU \\ hV \end{bmatrix} = \text{independent variable vector,} \\ F_i &= \begin{bmatrix} hU_i \\ hUU_i + \delta_{1i} \frac{1}{2}g(h^2 - H^2) \\ hVU_i + \delta_{2i} \frac{1}{2}g(h^2 - H^2) \end{bmatrix} = \text{convective flux vector,} \\ G_i &= \begin{bmatrix} 0 \\ -(h/\rho)\bar{\tau}_{1i} \\ -(h/\rho)\bar{\tau}_{2i} \end{bmatrix} = \text{diffusion fluxes,} \\ Q &= \begin{bmatrix} 0 \\ -h\hat{f}V - g(h - H)\frac{\partial H}{\partial x} - \frac{h}{\rho}\frac{\partial P_a}{\partial x} - \frac{1}{\rho}\tau_{31}^s + c_f \cdot U\sqrt{U^2 + V^2} \\ h\hat{f}U - g(h - H)\frac{\partial H}{\partial y} - \frac{h}{\rho}\frac{\partial P_a}{\partial y} - \frac{1}{\rho}\tau_{32}^s + c_f \cdot V\sqrt{U^2 + V^2} \end{bmatrix} = \text{source terms.} \end{aligned}$$

For a general shallow water flow, the value of the stress $\bar{\tau}_{ji}$, the surface stress τ_{ij}^s , the bottom stress τ_{ij}^b , and the atmospheric pressure gradient $\partial P_a/\partial x_i$ are very small and can be neglected, so the shallow water equations can be simplified as

$$\frac{1}{c^2} \frac{\partial p}{\partial t} + \frac{\partial U_i}{\partial x_i} = 0, \quad \frac{\partial U_i}{\partial t} + \frac{\partial}{\partial x_j}(u_j U_i) + \frac{\partial p}{\partial x_i} + Q = 0, \tag{15}$$

with

$$\begin{aligned} U_i &= \text{average velocity over the depth,} \\ p &= \frac{1}{2}(h^2 - H^2) = \text{pressure,} \\ c &= \sqrt{gh} = \text{wave celerity,} \\ Q &= -g(h - H)\frac{\partial H}{\partial x_i} + f_i = \text{source term,} \end{aligned}$$

in which f_i is the Coriolis force.

3. Review on characteristic-based split method

The numerical method used in this study is the characteristic-based split (CBS) algorithm, which was first proposed by Zienkiewicz and Codina [1995]. It can be applied to solve both compressible and incompressible flows, and is efficient and accurate. The main concept of this method is to split the shallow water equations into two parts:

- A set of simple scalar equations of convective-diffusion type that can be solved using a much bigger time step.
- A set of equations that are self-adjoint and can be discretized optimally by the Galerkin procedure, which can be solved implicitly and is unconditionally stable.

3.1. CBS time discretization. The time discretization in this scheme will treat the pressure gradient of the momentum equation (15)₂ as a source term, and will evaluate it differently in $t = t^n + \theta \Delta t$ at time increments Δt as shown below:

$$\frac{\partial p^{n+\theta_2}}{\partial x_i} = (1 - \theta_2) \frac{\partial p^n}{\partial x_i} + \theta_2 \frac{\partial p^{n+1}}{\partial x_i}. \tag{16}$$

This equation yields

$$\begin{aligned} \Delta U_i = \Delta t \left[-\frac{\partial}{\partial x_j} (u_j U_i) - Q + \frac{\Delta t}{2} u_k \frac{\partial}{\partial x_k} \left(\frac{\partial}{\partial x_j} (u_j U_i) + Q \right) \right]^n \\ - (1 - \theta_2) \Delta t \left[\frac{\partial p}{\partial x_i} - \frac{\Delta t}{2} u_k \frac{\partial}{\partial x_k} \left(\frac{\partial p}{\partial x_i} \right) \right]^n - \theta_2 \Delta t \left[\frac{\partial p}{\partial x_i} \right]^{n+1}. \end{aligned} \tag{17}$$

This can be split into two parts:

$$\Delta U_i = \Delta U_i^* + \Delta U_i^{**}, \tag{18}$$

where

$$\Delta U_i^* = \Delta t \left[-\frac{\partial}{\partial x_j} (u_j U_i) - Q + \frac{\Delta t}{2} u_k \frac{\partial}{\partial x_k} \left(\frac{\partial}{\partial x_j} (u_j U_i) + Q \right) \right]^n, \tag{19}$$

$$\Delta U_i^{**} = -(1 - \theta_2) \Delta t \left[\frac{\partial p}{\partial x_i} - \frac{\Delta t}{2} u_k \frac{\partial}{\partial x_k} \left(\frac{\partial p}{\partial x_i} \right) \right]^n - \theta_2 \Delta t \left[\frac{\partial p}{\partial x_i} \right]^{n+1} \tag{20}$$

$$= -\Delta t \left[\frac{\partial p^n}{\partial x_i} + \theta_2 \frac{\partial \Delta p}{\partial x_i} \right] + (1 - \theta_2) \frac{\Delta t^2}{2} u_k \frac{\partial}{\partial x_k} \frac{\partial p^n}{\partial x_i}, \tag{21}$$

$$\Delta p = p^{n+1} - p^n. \tag{21}$$

With the same procedure, the shallow water continuity equation can also be discretized in time as

$$\left(\frac{1}{c^2} \right)^n \Delta p = -\Delta t \left[\frac{\partial U_i}{\partial x_i} + \theta_1 \frac{\partial \Delta U_i}{\partial x_i} \right] = -\Delta t \left[\frac{\partial U_i}{\partial x_i} + \theta_1 \frac{\partial \Delta U_i^*}{\partial x_i} + \theta_1 \frac{\partial \Delta U_i^{**}}{\partial x_i} \right]. \tag{22}$$

Neglecting third-order terms, this can be written as

$$\left(\frac{1}{c^2} \right)^n \Delta p = -\Delta t \left[\frac{\partial U_i}{\partial x_i} + \theta_1 \frac{\partial \Delta U_i^*}{\partial x_i} - \Delta t \theta_1 \left(\frac{\partial^2 p^n}{\partial x_i \partial x_i} + \theta_2 \frac{\partial^2 \Delta p}{\partial x_i \partial x_i} \right) \right]. \tag{23}$$

This algorithm can be applied to both explicit and semiimplicit schemes, and depends on the selection of the values θ_1 and θ_2 . The stability criteria will depend on the scheme selected. For the fully explicit scheme, we have

$$1/2 \leq \theta_1 \leq 1, \quad \theta_2 = 0. \tag{24}$$

Stability is obtained when the time increment is less than the time limit, defined as

$$\Delta t \leq \Delta t_\sigma = \frac{a}{c + |u|}, \tag{25}$$

where

$$a = \text{element size}, \quad c = \sqrt{g \cdot h} = \text{wave celerity}, \quad |u| = \sqrt{U_i U_i}.$$

In semiimplicit form, the quantities of θ_1 and θ_2 are defined as

$$1/2 \leq \theta_1 \leq 1, \quad 1/2 \leq \theta_2 \leq 1. \tag{26}$$

This algorithm is conditionally stable. Three time limits have to be considered to assure stability:

$$\Delta t \leq \Delta t_\sigma = \frac{a}{|u|}, \quad \Delta t \leq \Delta t_\nu = \frac{a^2}{2\nu}, \quad \Delta t \leq \frac{\Delta t_\sigma \cdot \Delta t_\nu}{\Delta t_\sigma + \Delta t_\nu}, \tag{27}$$

where $\nu =$ kinematic viscosity.

3.2. CBS spatial discretization. The finite element methods (FEM) is used to discretize the space. FEM is an approximate method for solving differential equations of boundary and initial value problems. The basic concept of FEM is to divide a continuum into many smaller elements of convenient shapes—triangle, quadrilateral, and so on. Choosing suitable points (‘nodes’) within the elements, the variable in the differential equation is written as a linear combination of appropriately selected interpolation functions describing the variable. The governing equations are then transformed into a set of *finite element equations* for each element, and assembled into a global system based on the connectivity of the nodes. The nodal values of the variable are determined from this system of equations.

The spatial discretizations used in these formulations are

$$U_i = N(\bar{U}_i), \quad \Delta U_i = \Delta U_i^* + \Delta U_i^{**} = N(\Delta \bar{U}_i^*) + N \cdot (\Delta \bar{U}_i^{**}), \quad p = N \cdot (\bar{p}), \tag{28}$$

where

$$\begin{aligned} \bar{U}_i &= [\bar{U}_i^1 \ \bar{U}_i^2 \ \dots \ \bar{U}_i^k] = \text{Nodal velocities of a } k\text{-node element,} \\ N_i &= [N^1 \ N^2 \ \dots \ N^k] = \text{Galerkin shape function of a } k\text{-node element.} \end{aligned}$$

Equations (19), (20) and (23) are then discretized in space using the standard Galerkin finite element method. By writing the pressure p in terms of total water height h , these equations can be solved in three steps, as illustrated by Figure 3.

STEP 1

$$\mathbf{K}_1 \{ \Delta U_i^* \} = \mathbf{F}_1 (U_i^n, h^n, \Delta t)$$

$$\begin{bmatrix} \text{Diagonal Matrix} \end{bmatrix} \begin{Bmatrix} \Delta U^* \\ \Delta V^* \end{Bmatrix} = \begin{Bmatrix} \mathbf{F}u^* \\ \mathbf{F}v^* \end{Bmatrix}$$

Diagonal Matrix

STEP 3

$$\mathbf{K}_3 \{ \Delta U_i^{**} \} = \mathbf{F}_3 (U_i^n, h^n, h^{n+1}, \Delta t, \theta_2)$$

$$\begin{bmatrix} \text{Diagonal Matrix} \end{bmatrix} \begin{Bmatrix} \Delta U^{**} \\ \Delta V^{**} \end{Bmatrix} = \begin{Bmatrix} \mathbf{F}u^{**} \\ \mathbf{F}v^{**} \end{Bmatrix}$$

Diagonal Matrix

STEP 2

$$\mathbf{K}_2 (h^n, \Delta t, \theta_1, \theta_2) \{ \Delta h \} = \mathbf{F}_2 (\Delta U_i^*, \Delta U_i^n, h^n, \Delta t, \theta_1)$$

$$\begin{bmatrix} \text{Band Matrix} \end{bmatrix} \begin{Bmatrix} \Delta h \end{Bmatrix} = \begin{Bmatrix} \mathbf{F}h \end{Bmatrix}$$

$h^{n+1} = h^n + \Delta h$

Figure 3. CBS solution algorithm.

Step 1: Intermediate momentum equation. We have

$$\int_{\Omega} N \cdot \Delta U_i^* d\Omega = \Delta t \left[- \int_{\Omega} N \frac{\partial}{\partial x_j} (u_j U_i) d\Omega - \int_{\Omega} N \cdot Q_i d\Omega - \frac{\Delta t}{2} \int_{\Omega} \frac{\partial}{\partial x_k} (u_k N) \frac{\partial}{\partial x_j} (u_j U_i) d\Omega + \frac{\Delta t}{2} \int_{\Omega} (u_k \cdot N) \frac{\partial Q_i}{\partial x_k} d\Omega + \frac{\Delta t}{2} \int_{\partial\Omega} (N \cdot u_k) \frac{\partial}{\partial x_j} (u_j U_i) n_k d\Gamma \right]^n, \quad (29)$$

whose solution is

$$\Delta \bar{U}_i^* = -M^{-1} \Delta t [C \cdot \bar{U} + \Delta t \cdot K_u \bar{U} - (f + \Delta t \cdot f_s) - \Delta t \cdot K_b], \quad (30)$$

where

$$\begin{aligned} M &= \int_{\Omega} N^T N d\Omega, & f &= \int_{\Omega} N^T Q d\Omega, \\ C &= \int_{\Omega} N^T \frac{\partial}{\partial x_j} (u_j N) d\Omega, & f_s &= -\frac{1}{2} \int_{\Omega} \frac{\partial}{\partial x_i} (u_i N^T) Q d\Omega, \\ K_u &= \frac{1}{2} \int_{\Omega} \frac{\partial}{\partial x_k} (u_k N^T) \frac{\partial}{\partial x_j} (u_j N) d\Omega, & K_b &= \frac{1}{2} \int_{\partial\Omega} (u_k N^T) \frac{\partial}{\partial x_j} (u_j N) n_k d\Gamma. \end{aligned}$$

Step 2: Total water depth calculation.

$$\begin{aligned} & \int_{\Omega} N(\Delta h)d\Omega + \Delta t^2\theta_1\theta_2 \int_{\Omega} \frac{\partial N}{\partial x_i}(\tilde{c}^2) \frac{\partial(\Delta h)}{\partial x_i}d\Omega \\ &= -\Delta t \left[\int_{\Omega} N \frac{\partial U_i^n}{\partial x_i}d\Omega + \theta_1 \int_{\Omega} \frac{\partial N}{\partial x_i} \left(\Delta U_i^* - \Delta t(c^2)^n \frac{\partial h^n}{\partial x_i} \right) d\Omega \right. \\ & \quad \left. - \theta_1 \int_{\partial\Omega} N \left[\Delta U_i^* - \Delta t \left((c^2)^n \frac{\partial h^n}{\partial x_i} + \theta_2(\tilde{c}^2) \frac{\partial(\Delta h)}{\partial x_i} \right) \right] n_i d\Gamma \right], \end{aligned} \quad (31)$$

whose solution is

$$\begin{aligned} \Delta \bar{h} &= (\tilde{M} + \Delta t^2 \cdot \theta_1\theta_2\tilde{c}^2(H - Q_b))^{-1} \Delta t \\ & \quad \times \left[Q(-\bar{U}_i + \theta_1\Delta \bar{U}_i^*) - \Delta t\theta_1c^2H \cdot \bar{h} + \theta_1(\Delta t \cdot c^2Q_b\bar{h} - M_b\Delta \bar{U}_i^*) \right]^n, \end{aligned} \quad (32)$$

where

$$\begin{aligned} \tilde{M} &= \int_{\Omega} N^T N d\Omega, & M_b &= \int_{\partial\Omega} N^T N \cdot n_i \cdot d\Gamma, \\ Q &= \int_{\Omega} \frac{\partial N^T}{\partial x_i} N \cdot d\Omega, & H &= \int_{\Omega} \frac{\partial N^T}{\partial x_i} \frac{\partial N}{\partial x_i} \cdot d\Omega, & Q_b &= \int_{\partial\Omega} \frac{\partial N^T}{\partial x_i} N \cdot n_i d\Gamma. \end{aligned}$$

Step 3: Velocity correction.

$$\begin{aligned} \int_{\Omega} N \Delta U_i^{**} d\Omega &= -\Delta t \cdot (1 - \theta_2) \int_{\Omega} N(c^2)^n \frac{\partial h^n}{\partial x_i} d\Omega - \Delta t\theta_2 \int_{\Omega} N(c^2)^{n+1} \frac{\partial h^{n+1}}{\partial x_i} d\Omega \\ & \quad - (1 - \theta_2) \frac{\Delta t^2}{2} \int_{\Omega} \frac{\partial N}{\partial x_k} u_k \left((c^2)^n \frac{\partial h^n}{\partial x_i} \right) d\Omega - (1 - \theta_2) \frac{\Delta t^2}{2} \int_{\Omega} N \frac{\partial u_k}{\partial x_k} \left((c^2)^n \frac{\partial h^n}{\partial x_j} \right) d\Omega \\ & \quad + (1 - \theta_2) \frac{\Delta t^2}{2} \int_{\partial\Omega} N u_k \left((c^2)^n \frac{\partial h^n}{\partial x_j} \right) \cdot n_i \cdot d\Gamma. \end{aligned} \quad (33)$$

The solution of Equation (33) is

$$\Delta(\bar{U}_i)^{**} = -M \cdot^{-1} \Delta t \cdot \left[Q^T [(1 - \theta_2)(c^2)^n \bar{h}^n + \theta_2(c^2)^{n+1} \bar{h}^{n+1}] + \frac{\Delta t}{2} P(c^2)^n \bar{h}^n - \frac{\Delta t}{2} P_b(c^2)^n \bar{h}^n \right], \quad (34)$$

where

$$\begin{aligned} M &= \int_{\Omega} N^T N d\Omega, & P &= (1 - \theta_2) \int_{\Omega} \frac{\partial}{\partial x_i} (u_i N^T) \frac{\partial N^T}{\partial x_i} d\Omega, \\ Q &= \int_{\Omega} \frac{\partial N^T}{\partial x_i} N \cdot d\Omega, & P_b &= (1 - \theta_2) \int_{\partial\Omega} (u_k N^T) \frac{\partial N^T}{\partial x_i} n_k d\Gamma, \end{aligned}$$

and where $i, j, k = 1, 2$, and N is the standard finite element shape function. The variable \tilde{c} is the average value of the celerity over the time step, while Ω is the flow domain bounded by $\partial\Omega$, and n_k is the outward normal of the boundary $\partial\Omega$. Step 1 and Step 3 can be solved explicitly, while Step 2 needs to be solved implicitly. The velocity is computed in two stages by the characteristic Galerkin method as shown in Step 1 and Step 3. In Step 2, the pressure, or elevation of the free surface, is solved from a

self-adjoint Laplacian-type equation, which can be discretized optimally by the Galerkin procedure. In this semiimplicit form, the algorithm's time step depends only on the current velocity, rather than on the wave celerity. By now it should be clear why the CBS method is very efficient.

4. Review on exact solution

The exact solution for water elevation is achieved by solving the continuity equation above. By defining η as the water elevation, we can get

$$\eta(x, t) = \frac{H}{2} \cos(kx - \sigma t), \tag{35}$$

where

$$k = \frac{2\pi}{L} = \text{the wave number}, \tag{36}$$

$$\sigma^2 = \frac{2\pi}{T} = gk * \tanh(kh) = \text{the circular frequency}, \tag{37}$$

$$c = \frac{\sigma}{k} = \frac{2\pi/T}{2\pi/L} = \frac{L}{T} = \text{the wave celerity}. \tag{38}$$

For shallow water waves, where kh is very small ($kh < \pi/10$), the hyperbolic function $\tanh(kh)$ can be approximated as kh . With this simplification, the dispersion relationship for shallow water reduces in such a way that the wave celerity for shallow water wave can be defined as

$$\sigma^2 = gk * \tanh(kh) = gk^2h, \quad \frac{\sigma^2}{k^2} = c^2 = gh, \quad c = \sqrt{gh}. \tag{39}$$

From the linearized frictionless momentum equations, we have

$$\frac{\partial U}{\partial t} = -g \frac{\partial \eta}{\partial x}. \tag{40}$$

Substituting Equation (35) into Equation (40), we get

$$\frac{\partial U}{\partial t} = g \frac{H}{2} k \sin(kx - \sigma t),$$

or

$$U = g \frac{H}{2\sigma} k \cos(kx - \sigma t) = \frac{c}{h} \eta. \tag{41}$$

If we further examine the change in wave height due to changes in water depth and channel width, we find that

$$H_2 = H_1 \left(\frac{h_1}{h_2} \right)^{1/4} \left(\frac{b_1}{b_2} \right)^{1/2}, \tag{42}$$

where subscript 1 indicates the location at the reference point, and subscript 2 indicates the location at the examined point. For a special case where the channel width is uniform ($b_1 = b_2$), this relationship is called Green's Law. This formula implies that a change in water depth or channel width can change the water height.

5. Model verification and demonstration

The element used in this study is a standard linear triangular element with three unknowns to be solved in each node, as shown in Figure 4. These unknowns are h , U , and V which determine the water elevation and the mass flow in x and y directions. The area and line integrations are calculated numerically using one Gauss point, as show in Figure 5.

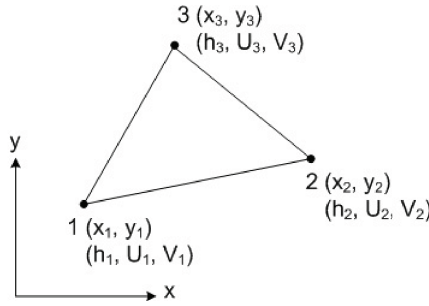


Figure 4. Triangular element.

The wave parameters will be defined based on the characteristic of shallow water wave states where the ratio of the vertical scale h to the horizontal scale L is very small. Our shallow water condition is:

$$h/L < 0.05 \quad \text{or} \quad kh < \pi/10. \tag{43}$$

In this study, water depth is kept constant at the level $h = 0.5$ m. Using this water depth, we can compute the wave celerity simply by using Equation (39):

$$c = \sqrt{gh} = 2.214 \text{ m/s}. \tag{44}$$

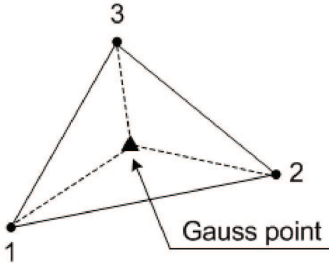
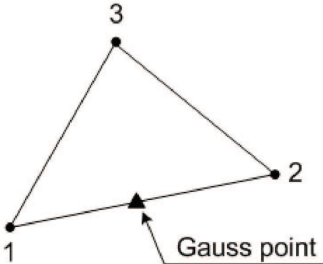
Numerical Area integration	Numerical Line integration
 $\int_{\Omega} N_1 d\Omega = \int_{\Omega} N_2 d\Omega = \int_{\Omega} N_3 d\Omega = \frac{1}{3} * \text{Area}$	 $\int_{\partial\Omega} N_1 d\Gamma = \int_{\partial\Omega} N_2 d\Gamma = \frac{1}{2} * \text{Length}$ $\int_{\partial\Omega} N_3 d\Gamma = 0$

Figure 5. Numerical integration.

Parameter:	Symbol	Value used
Water depth	H	0.5 m
Wave amplitude	A	0.02 m
Wave period	T	10 s
Time stepping parameter	θ_1 and θ_2	0.5
Time increment	Δt	0.0625 s
Lumping parameter	B	0.9

Table 1. Parameters used in this study.

Using Equations (36) and (38) with $k = 2\pi/L$ and $L = c \cdot T$, we can compute the wave period by

$$kh < \frac{\pi}{10} \rightarrow \frac{2\pi}{c \cdot T}h < \frac{\pi}{10} \rightarrow T > 4.52 \text{ s.} \tag{45}$$

To satisfy this condition, the wave period is set to 10 s, and the wave amplitude is set at 0.02 m. The wavelength is computed using Equation (38) and is equal to 22.14 m. For the sake of stability, the time stepping parameters θ_1 and θ_2 are set to 0.5, following the Crank–Nicolson scheme. The time step increment, Δt , is set to be 0.0625 s, and the lumping parameter β is set at 0.9. These parameters, used throughout this study, are summarized in Table 1.

The model will be verified and demonstrated by solving and analyzing four case studies. The analysis is done by performing a convergence test and, where possible, comparing the numerical results with exact solutions and laboratory experiments. In cases where the exact solution is not available, the analysis is based only on the physical characteristics of the water flow. These cases serve as demonstrations of the capability of the model.

Case 1: Flow in rectangular channel with constant depth. A simple experiment of shallow water wave propagation is done in a frictionless channel with a length and depth of 50 m and 10 m respectively. The purpose of this case is to verify that the FEM solution for water elevation, velocity, and pressure converge well as our mesh gets finer. Other wave parameters will also be verified.

A series of waves are generated on one side, such that they will propagate to the other side and reflect back. The boundary conditions we apply to the model are the normal velocity on the boundary B-C, C-D, and A-D is assumed to be zero, while a sinusoidal wave is imposed on the boundary A-B with an amplitude of 0.02 m and a period of 10 s.

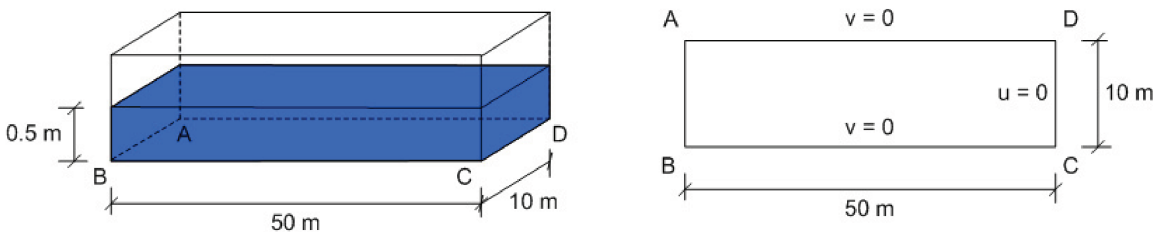


Figure 6. Rectangular profile with constant depth.

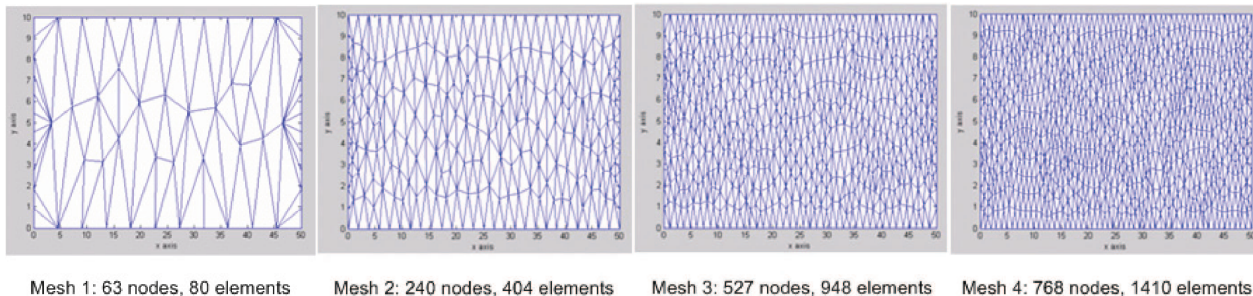


Figure 7. Four types of mesh used in Case 1.

We will study convergence of solutions across four successively refined meshes, as shown in Figure 7. The convergence test is conducted at regular 5 m intervals within the channel. Figure 8 compares water elevations in the FEM and exact solutions, at time = 20 s and $x = 5, 10, 15, 20, 25$ and 30 m.

Looking to Figure 8, we see that the FEM solution using meshes 2, 3, and 4 give results close to the exact solution. The exact solution given here is for a wave in a steady state. Looking to our results, the error seems to be increasing as x increases. This can be explained by the fact that, when the wave is generated, it will first propagate in a transient state, only reaching the steady state after quite some time. Furthermore, the exact solution gives no wall boundary condition around the channel. If we look at the steady state region, $x \leq 15$ m, the FEM with mesh 4 gives pretty good results. By contrast, at $x = 50$ m we see a clear difference between the FEM and exact solutions. The wave in the numerical solution has yet to arrive, while the wave in the exact solution is already in its steady state. Results from successively refined meshes do not converge very well, and sometimes the least error is found with a mesh other than mesh 4, which is the most refined mesh. This is likely the result of the irregular shape and location of the triangles used in the meshing scheme.

To further confirm our method, we examine the accuracy of the physical results got using mesh 4. Looking to Figure 9, which shows the wave at time = 25 s, we see that the amplitude of the wave

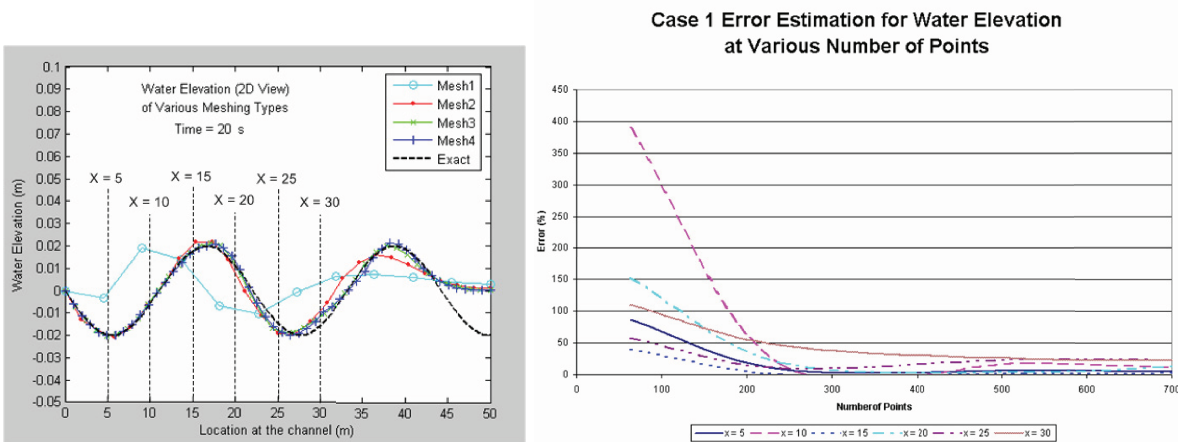
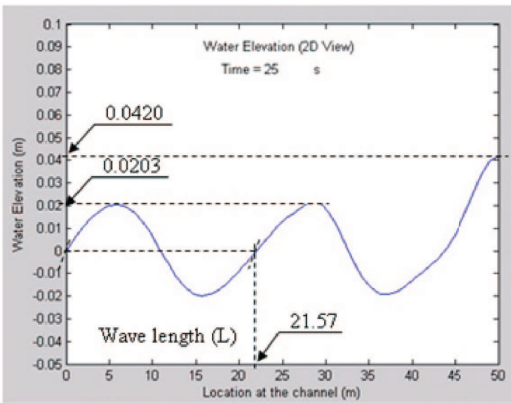


Figure 8. Water elevation result of Case 1 at time = 20 s.



	FEM	Exact	Error
Wave Length	21.57 m	22.14 m	2.58 %
Amplitude	0.0203 m	0.02 m	1.50 %
Maximum water elevation on the wall	0.0420 m	0.04 m	5.00 %

Figure 9. Wave properties at time = 25 s.

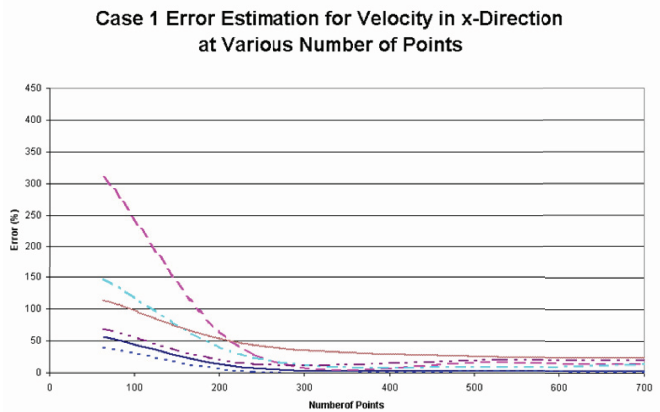
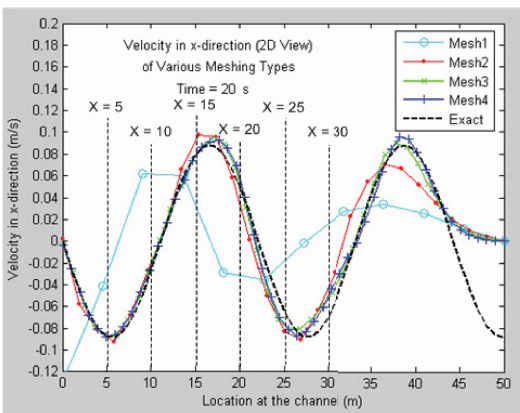


Figure 10. Velocity in x-direction of Case 1 at time = 20 s.

is consistently 0.0203 m. This is a 1.5% error relative to the initial amplitude of 0.02 m. The FEM wavelength is computed to be 21.57 m, which is 2.58% in excess of the exact solution 22.14 m. When the wave hits the wall (at time ≈ 25 s), the maximum water elevation will double, to 0.04 m. The FEM solution gives this elevation as 0.0420 m, a 5.00% error.

Since the water pressure is derived directly from water elevation ($p = 0.5g(h^2 - H^2)$), it has exactly the same behavior as water elevation. The velocity in the x -direction for both FEM and exact solutions at time = 20 s are presented in Figure 10. The convergence test is again conducted at the same 5 m intervals.

The behavior of the velocity is similar to that of the water elevation. FEM solutions of velocity using meshes 3 and 4 give results close to the exact solution in the steady state region, $x < 15$ m. Velocity in the y -direction is zero for all time throughout the channel. This is as expected, as the imposed wave is symmetrical. Again, the results converge poorly due to the irregular triangular meshing. The maximum velocity in the x -direction is 0.0952 m/s which has 7.25% error from exact solution 0.0883 m/s.

Case 2: Flow in rectangular channel with irregular depth. Next, we pursue a variation on Case 1, a rectangular channel with irregular depth as shown in Figure 11. Again, we assume no normal velocity

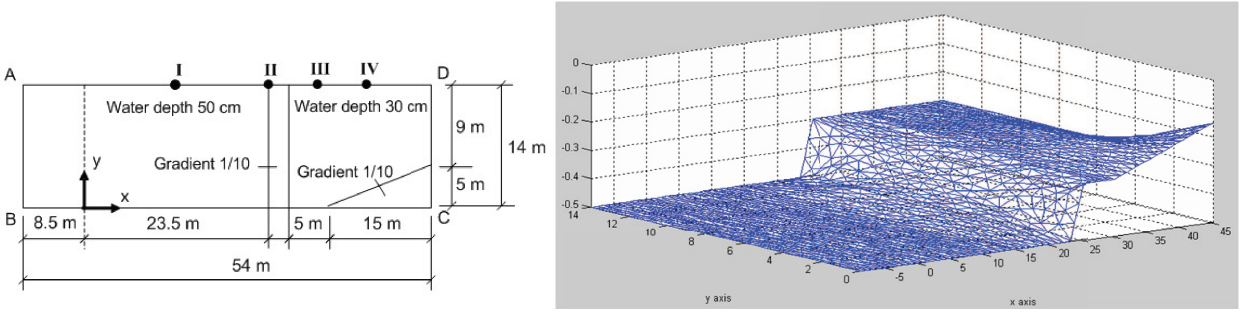


Figure 11. Channel profile of Case 2.

along boundaries B-C, C-D, and A-D, with a sinusoidal wave imposed on boundary A-B. The wave's amplitude is 0.02 m and its period of 10 s. The water elevation will be computed on the edge of the channel ($y = 14$ m) at four different points ($x_I = 11.5$ m, $x_{II} = 23.5$ m, $x_{III} = 29.5$ m, and $x_{IV} = 35.5$ m).

We compare the results of this case study with experimental data, and other numerical result previously done by Cheng and Kawahara [1991] using the combination of the explicit and quasi explicit standard Galerkin finite element method.

The water elevations at our four reference points are plotted against time in Figure 12. The dotted line shows observed experimental data, the solid line shows the numerical result using the standard Galerkin finite element method, and the dashed line is the numerical result using the CBS method. From the figure

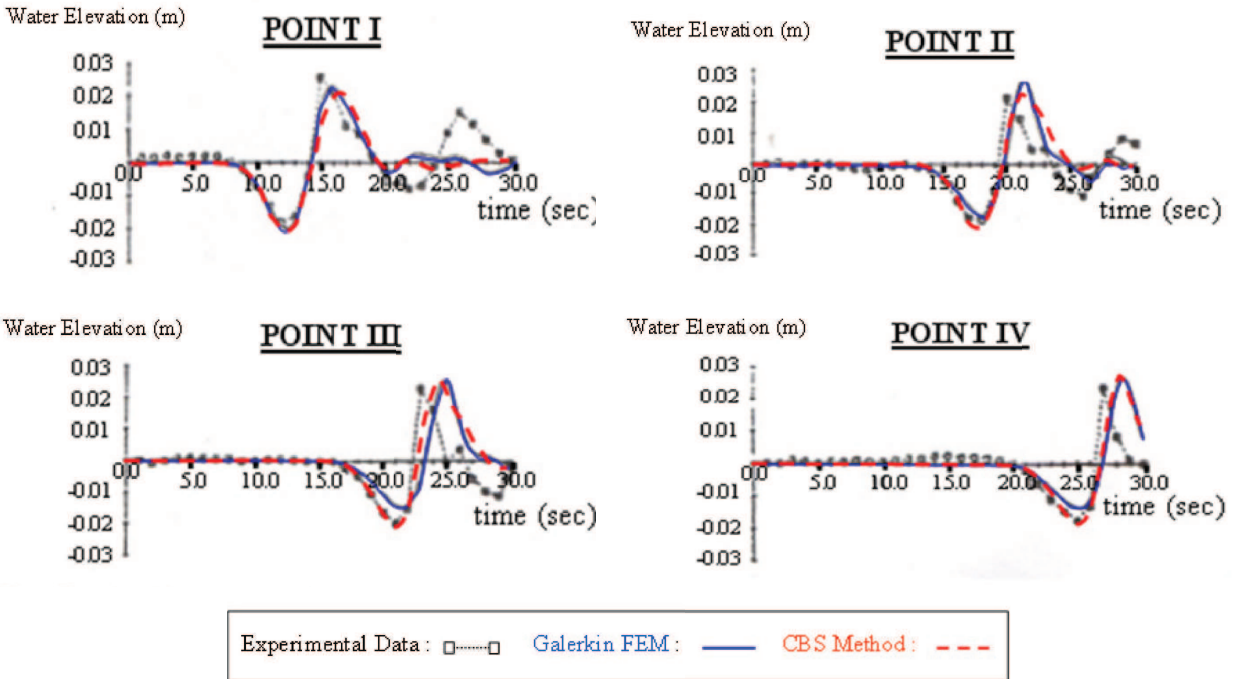


Figure 12. Numerical results of Case 2.

we see that the values obtained using the CBS method are the better of the numerical results, closer to the experimental data.

Snapshots of the three-dimensional view of water elevation are shown in Figure 13. From the simulation, it can be seen that when the wave enters the shallower area, its height increases. This corresponds with the characteristic of tsunami propagation.

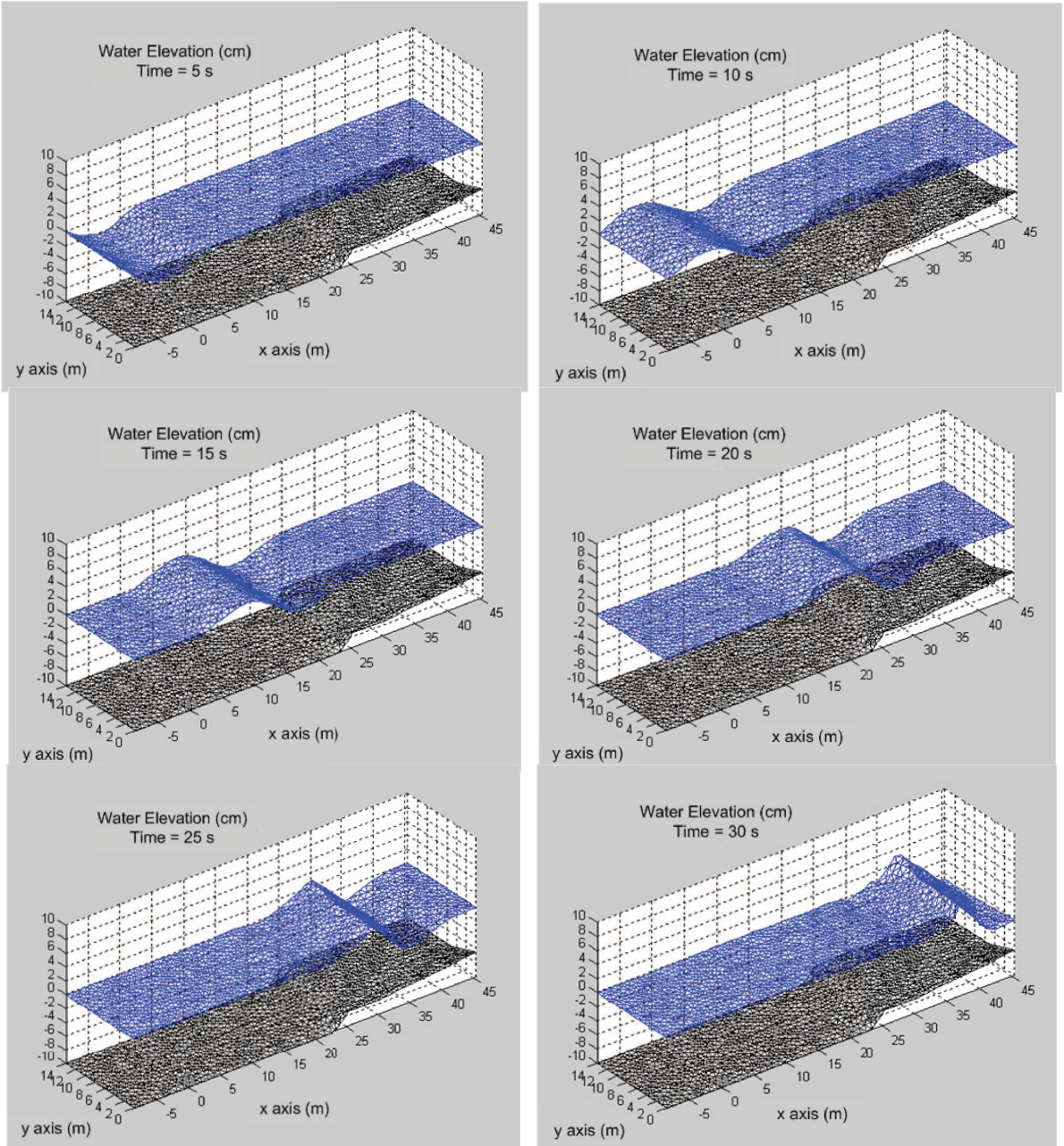


Figure 13. Water elevation of Case 2 at various time steps.

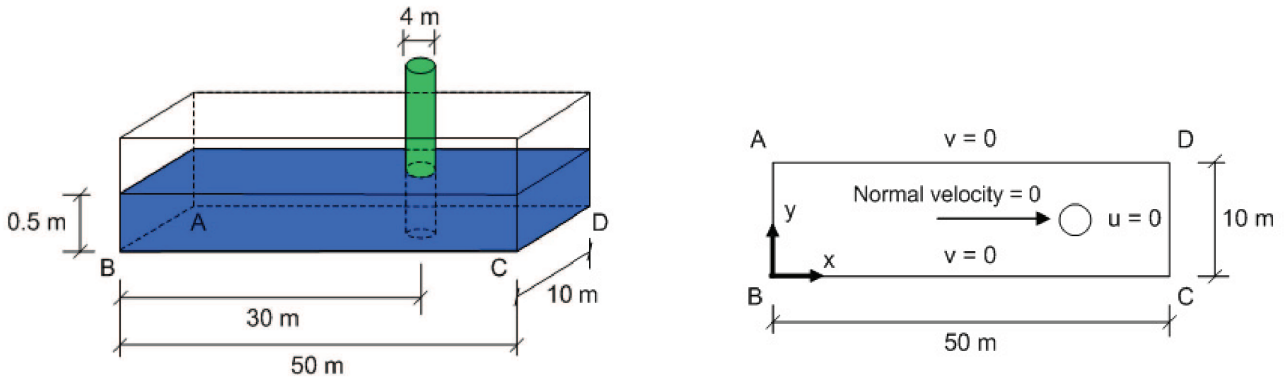


Figure 14. Channel profile for Case 3.

Case 3. Flow passing a solid barrier. In Case 3, a cylindrical barrier with a diameter of 4 m is placed in the middle of the channel at $x = 30$ m, as shown in Figure 14. The purpose of this case is to model and study the behavior of the tsunami wave passing a solid barrier, such as an offshore structure. Again, we set the normal velocity along boundaries B-C, C-D, and A-D to zero, and propagate a sinusoidal wave with an amplitude of 0.02 m and a period of 10 s from boundary A-B.

Snapshots of the wave's elevation at two times are plotted in Figure 15. The solid lines show the water elevation in the middle of the channel ($y = 5$ m), while the dashed lines show the water elevation in the edge of the channel ($y = 0$ m).

If we look at Figure 15, at time $t = 15$ s there is a difference in water elevation between the water in the middle of the channel ($y = 5$ m), which starts to hit the barrier, and the water on the edge of the channel ($y = 0$ m), which still propagates with the same amplitude. At time $t = 25$ s, the maximum water elevation at the wall is about 0.035 m. In Case 1 where there is no barrier, the maximum water

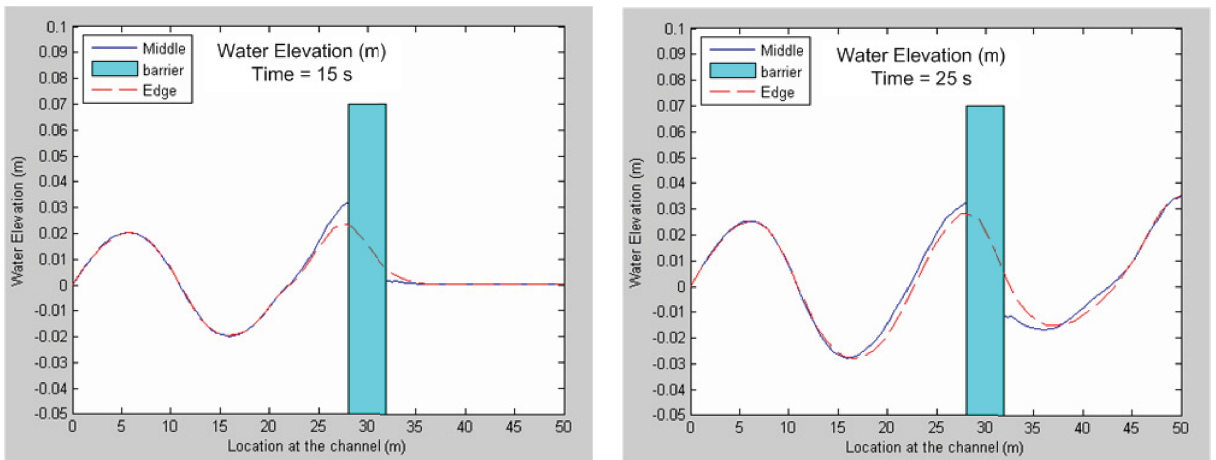


Figure 15. Water elevation of Case 3 at $t = 15$ s and $t = 25$ s.

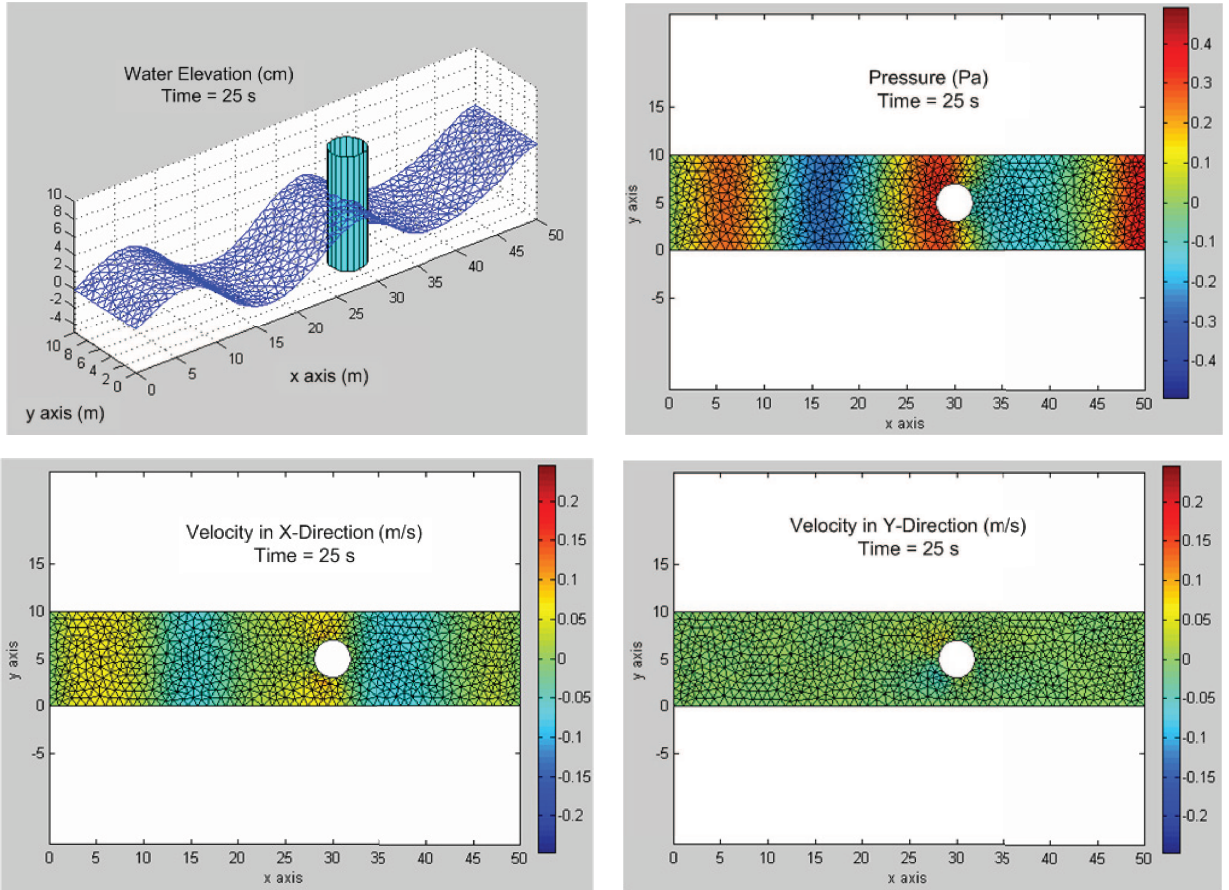


Figure 16. Water elevation, pressure, and velocity of Case 3 at $t = 25$ s.

elevation at the wall is 0.04 m. So in this case, it is shown that the barrier has reduced the maximum water elevation by up to 12.5%.

Figure 16 shows the water elevation as a three-dimensional view, along with water pressure and also velocity in x and y directions. From this figure, we can see that the velocity and pressure propagate in the same manner as the water elevation, which means the higher the water elevation, the higher the velocity and the pressure. The only difference appears at the wall boundary condition. The water elevation and pressure are maximized due to the reflecting wave, but the velocity is zero.

Case 4: Flow in circular channel with constant depth. Tsunami propagation due to an earthquake on the open sea is modeled using a circular channel with a diameter of 50 m and constant depth of 0.5 m, as shown in Figure 17. The land surrounding the sea is modeled by assuming the normal velocity around the channel to be zero. The earthquake is modeled by imposing a sinusoidal wave with amplitude of 0.02 m and period of 10 s in a small circular area with a radius of 1 m in the center of the channel.

Figure 18 represents the water elevation in the middle of the channel ($y = 0$ m) where we can see that the initial bottom deformation of 0.02 m generates an initial wave with amplitude of 0.02 m. The wave

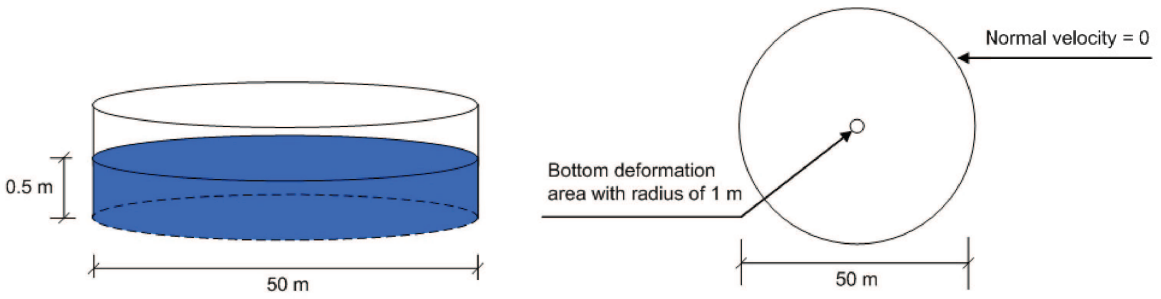


Figure 17. Channel profile of Case 4.

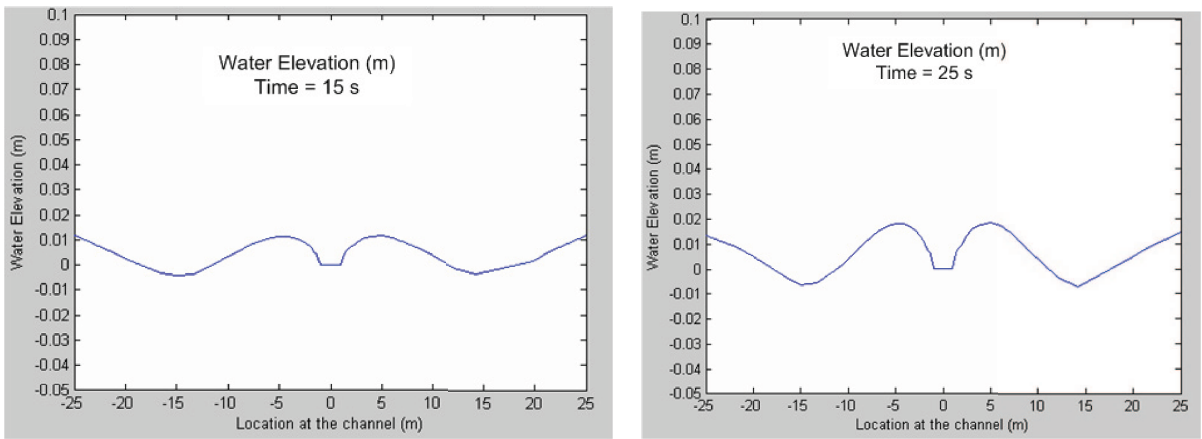


Figure 18. Water elevation of Case 3 in the middle of the channel ($y = 0$ m) at $t = 15$ s and $t = 215$ s.

then propagates symmetrically with a decreased amplitude. When the first wave reaches the wall around the circular channel, the maximum water elevation is only 0.012 m. This means that while propagating out to a radius of 25 m, the wave loses up to 70% of its height, or about 2.8% per meter travelled. Three-dimensional snapshots of the water elevation, pressure, and velocity are shown as Figure 19.

6. Tsunami simulation

In this section, we use the presented finite element method to model the propagation of the December 26, 2004 tsunami. Figure 20 presents the tsunami propagation model in the domain of 10° S – 20° N and 80° E – 100° E.

To be able to perform analysis of real tsunami propagation, appropriate wave sources for tsunamis must be employed. These wave sources will have to be derived from earthquakes that occur in the problem domain. An appropriate wave source model for tsunami propagation problems is still in development. To illustrate the capability of the present finite element model in predicting tsunami wave traveling time, our simulation uses a simple wave source in the form of sinusoidal wave with an amplitude of 1 m and period of 300 seconds.

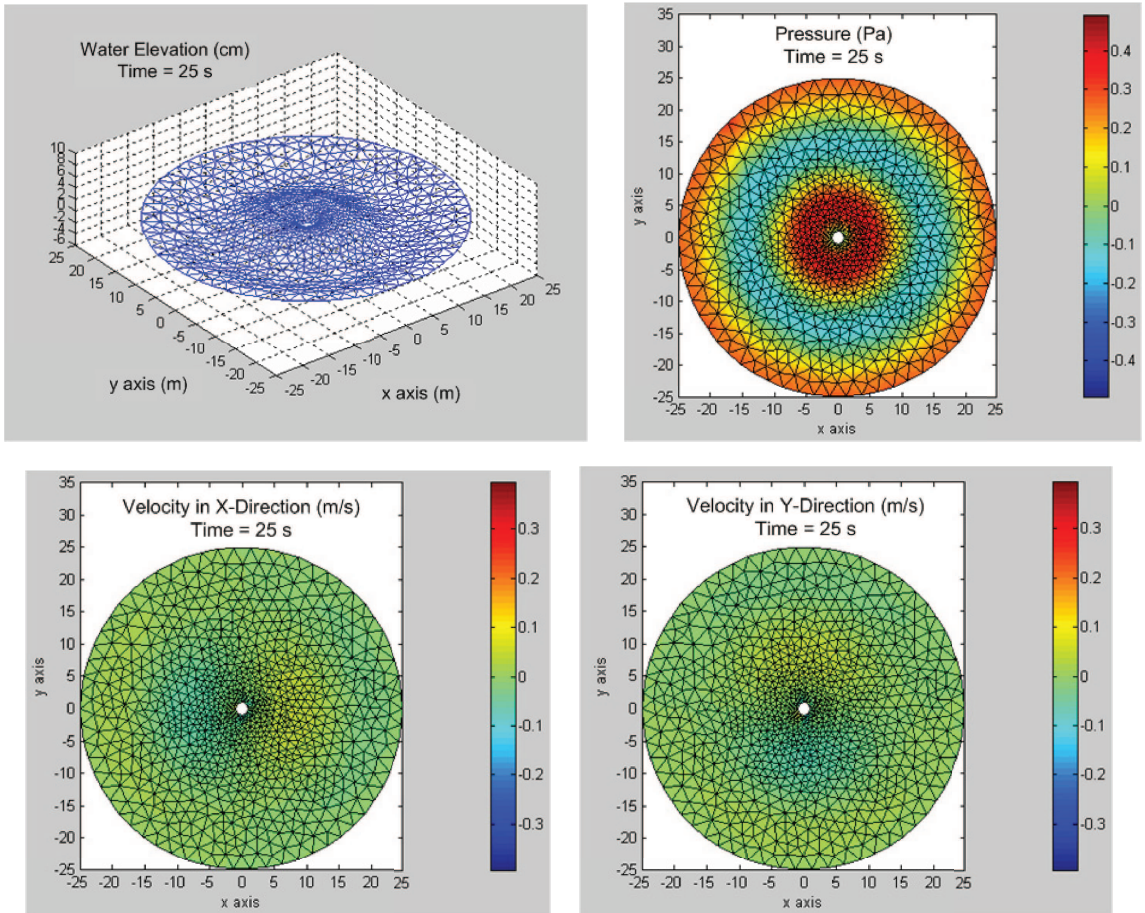


Figure 19. Water elevation, pressure, and velocity of Case 4 at $t = 25$ s.

Figure 21, left, shows the first simulation, estimating wave speed in deep water. In deep water, tsunami waves move at a speed that is equal to the square root of the product of the acceleration of gravity and the water depth. In the studied domain, with an average water depth of 6000 m, the analytical tsunami wave speed is calculated as 240 m/s. The simulation is conducted up to 6000 seconds with the sinusoidal wave at the left boundary as shown in the same figure. As derived from wave's ultimate translation, our model estimates a deep water tsunami wave speed of 225 m/s.

The second simulation serves as a tool to predict tsunami wave traveling time to the shoreline. The sinusoidal wave source is excited at the island shown in Figure 21, right. From numerical simulation, the time of tsunami wave traveling from the excited island to Phuket area in the figure is 1 hour and 14 minutes. The result is relatively close to the real observation obtained from the December 26, 2004 Tsunami. This important feature of the present model has been implemented in the Tsunami tracking and alert system currently under development at Thailand's Asian Institute of Technology, School of Engineering and Technology.

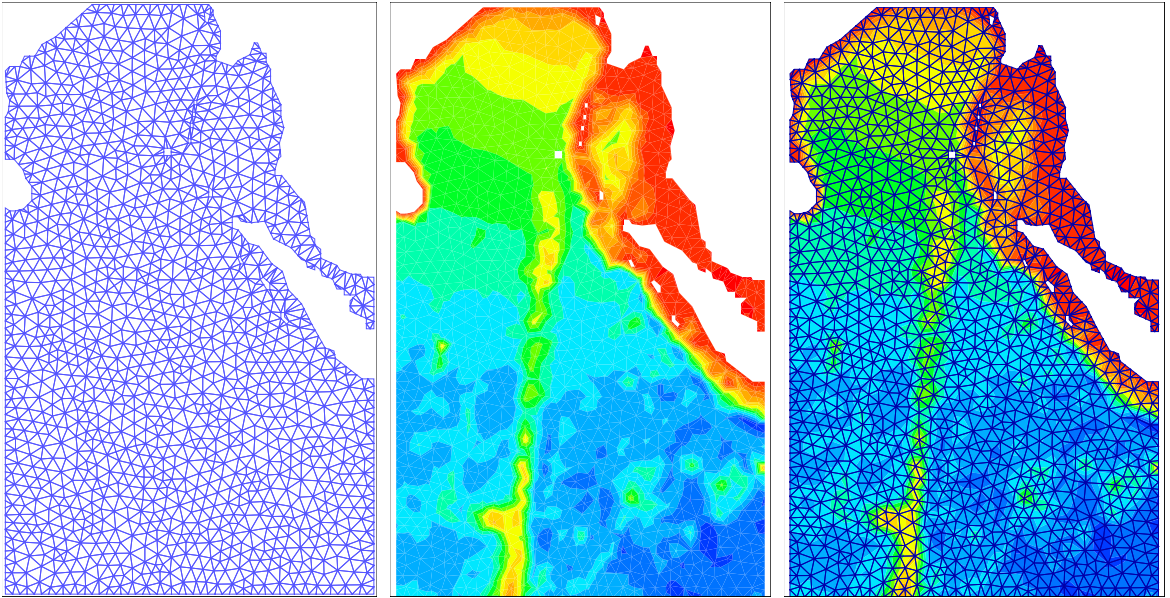


Figure 20. Finite element model for the propagation of the December 26, 2004 tsunami. Left: mesh created for the domain; middle: bathymetry data; right: composite of both.

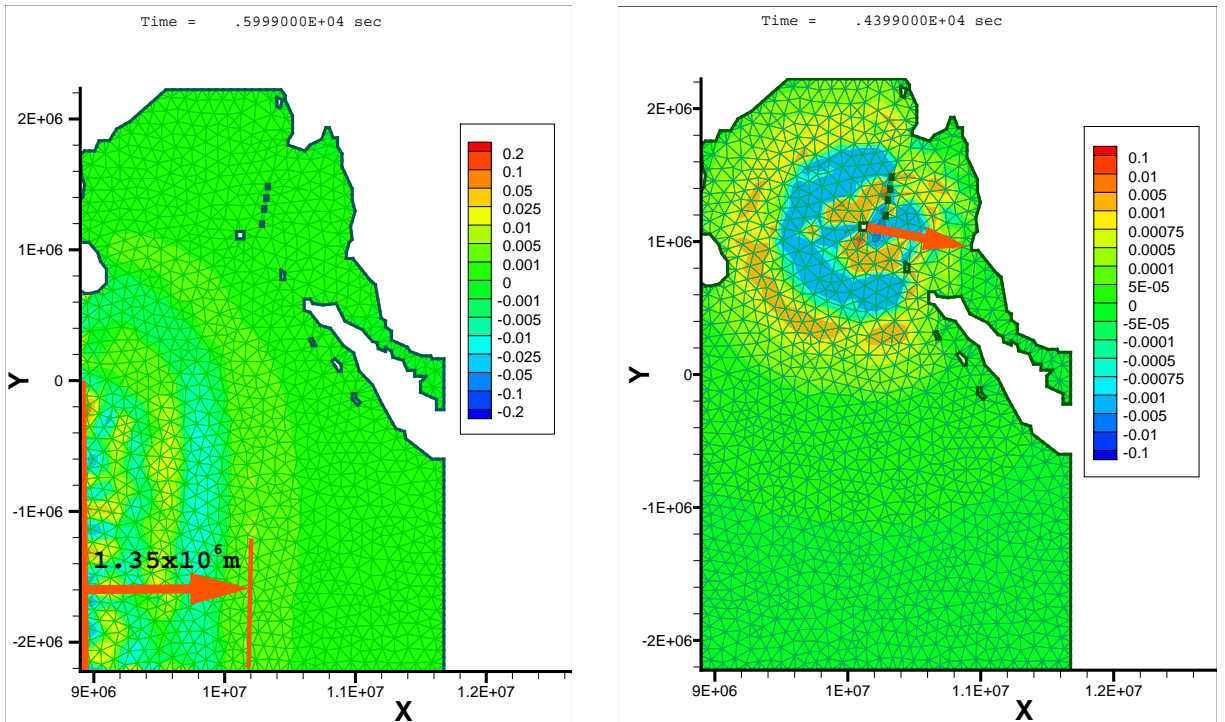


Figure 21. Estimating wave speed in deep water (left) and traveling time to shoreline (right). Labels are in meters.

7. Conclusions

This paper presented the characteristic-based split as a method for the solution of the shallow water equations. The main advantages of this method are its efficiency and accuracy. The efficiency is obtained from the split procedure, which enables us to solve some equations explicitly. From the numerical results in Case 2, it is shown that the CBS solution is very accurate, giving results closer to the experimental data than those given by the standard Galerkin method. The numerical model can also be used to model tsunami propagation passing a solid barrier, as shown in Case 3, and tsunami propagation due to an earthquake on the open sea, as shown in Case 4. Using these case studies, we showed the method's facility in modeling the characteristics of real tsunami propagation, namely that water elevation increases as a tsunami enters shallower areas, and that, in general, the higher the water elevation, the higher the water velocity and pressure. The exception to this correspondence between water velocity and water elevation appears at the wall boundary, where the water elevation doubles and the wave is reflected from the wall with zero velocity. Finally, the propagation of the December 26, 2004 tsunami is modeled using the CBS method. The numerical simulation gives relatively close results compared to actual data from the event. However, this correspondence is limited due to the lack of an appropriate wave source. The result using an arbitrary wave source is designed to illustrate the capability of the model, and motivate its use when appropriate wave sources can be supplied. This analysis of a truly real tsunami will be addressed in a future paper, after the development of a wave source model for tsunami propagation is complete.

Acknowledgement

The authors acknowledge the advice of R. L. Taylor and P. Nithiarasu on the coding of the CBS algorithm.

References

- [Cheng and Kawahara 1991] J. Y. Cheng and M. Kawahara, "Finite element method for shallow water wave analysis", pp. 1679–1683 in *Computational mechanics: Proceedings of the Asian Pacific Conference on Computational Mechanics* (Hong Kong, 1991), vol. 2, edited by Y. K. Cheung et al., Balkema, Rotterdam, 1991.
- [Gill 1982] A. E. Gill, *Atmosphere-ocean dynamics*, Academic Press, 1982.
- [Groen and Groves 1962] P. Groen and G. W. Groves, "Surges", pp. 611–646 in *The sea*, vol. I, edited by M. N. Hill, Interscience, 1962.
- [Grotkop 1973] G. Grotkop, "Finite element analysis of long-period water waves", *Comput. Methods Appl. Mech. Eng.* **2:2** (1973), 147–157.
- [Heaps 1967] N. S. Heaps, "Storm surges oceanography and marine biology", *Oceanogr. Mar. Biol.* **5** (1967), 11–47.
- [Houston 1978] J. R. Houston, "Interaction of tsunamis with the Hawaiian islands calculated by a finite-element numerical model", *J. Phys. Oceanogr.* **8:1** (1978), 93–102.
- [Imamura 1996] F. Imamura, "Review of tsunami simulation with a finite difference method", pp. 25–42 in *Long-wave runup models* (Friday Harbor, WA, 1995), edited by H. Yeh et al., World Scientific, Singapore, 1996.
- [Kawahara et al. 1978] M. Kawahara, N. Takeuchi, and T. Yoshida, "Two step explicit finite element method for tsunami wave propagation analysis", *Int. J. Numer. Methods Eng.* **12:2** (1978), 331–351.
- [Le Méhauté 1976] B. Le Méhauté, *An introduction to hydrodynamics and water waves*, Springer, New York, 1976. MR 57 #11286
- [Mader 2004] C. L. Mader, *Numerical modelling of water waves*, 2nd ed., CRC Press, Boca Raton, FL, 2004.

- [Malone and Kuo 1981] F. D. Malone and J. T. Kuo, “Semi-implicit finite element methods applied to the solution of the shallow water equations”, *J. Geophys. Res.* **86**:C5 (1981), 4029–4040.
- [Nithiarasu et al. 2004] P. Nithiarasu, J. S. Mathur, N. P. Weatherill, and K. Morgan, “Three-dimensional incompressible flow calculations using the characteristic based split (CBS) scheme”, *Int. J. Numer. Methods Fluids* **44**:11 (2004), 1207–1229. MR 2043786
- [Ortiz et al. 2004] P. Ortiz, O. C. Zienkiewicz, and J. Szmelter, “CBS finite element modelling of shallow water and transport problems”, in *European Congress on Computational Methods in Applied Sciences and Engineering* (Jyväskylä, 2004), edited by P. Neittaanmäki et al., University of Jyväskylä, Jyväskylä, 2004.
- [Peraire et al. 1986] J. Peraire, O. C. Zienkiewicz, and K. Morgan, “Shallow water problems: A general explicit formulation”, *Int. J. Numer. Methods Eng.* **22**:3 (1986), 547–574. MR 87e:76029
- [Sklarz et al. 1979] M. A. Sklarz, L. Q. Spielvogel, and H. G. Loomis, “Numerical simulation of the 29 November 1975 island of Hawaii tsunami by the finite-element method”, *J. Phys. Oceanogr.* **9**:5 (1979), 1022–1031.
- [Wei and Kirby 1995] G. Wei and J. T. Kirby, “Time-dependent numerical code for extended Boussinesq equations”, *J. Waterw. Port C. (ASCE)* **121**:5 (1995), 251–261.
- [Zienkiewicz and Codina 1995] O. C. Zienkiewicz and R. Codina, “A general algorithm for compressible and incompressible flow, I: The split, characteristic-based scheme”, *Int. J. Numer. Methods Fluids* **20**:8–9 (1995), 869–885. MR 96d:76060a
- [Zienkiewicz et al. 1999] O. C. Zienkiewicz, P. Nithiarasu, R. Codina, M. Vázquez, and P. Ortiz, “The characteristic-based-split procedure: An efficient and accurate algorithm for fluid problems”, *Int. J. Numer. Methods Fluids* **31**:1 (1999), 359–392. MR 2000g:76084

Received 15 Jun 2007. Revised 19 Feb 2008. Accepted 21 Feb 2008.

GUNAWAN BUDI WIJAYA: gunawan_sipil@yahoo.co.uk

School of Engineering and Technology, Asian Institute of Technology, P.O. Box 4 Klong Luang, Pathumthani 12120, Thailand

TAM THANH BUI: loantam@ait.ac.th

School of Engineering and Technology, Asian Institute of Technology, P.O. Box 4 Klong Luang, Pathumthani 12120, Thailand

WORSAK KANOK-NUKULCHAI: worsak@ait.ac.th

School of Engineering and Technology, Asian Institute of Technology, P.O. Box 4 Klong Luang, Pathumthani 12120, Thailand